Infrared Spectroscopy of the Amide I Mode of *N*-Methylacetamide in Solid Hydrogen at 2–4 K

Leif O. Paulson and David T. Anderson*

Department of Chemistry, University of Wyoming, Laramie, Wyoming 82071-3838, United States

Ⓢ *Supporting Information*

ABSTRACT: We report high-resolution ($0.05\ \mathrm{cm^{-1}}$) FTIR spectra of the fundamental and first overtone of the amide I mode of *trans-N*-methylacetamide (NMA) trapped in solid molecular hydrogen (SMH) at cryogenic temperatures with low (0.03%) and high (55%) *ortho*-hydrogen (oH_2) concentrations. NMA-doped SMH samples with high oH_2 concentrations are nearly free from inhomogeneous broadening, permitting the measured amide I homogeneous line width of $1.268(8)\ \mathrm{cm^{-1}}$ to be used to place a lower limit on the vibrational lifetime of $4.19(3)$ ps. Direct observation of the amide I overtone allows the harmonic vibrational frequency $\omega_e = 1726.6(5)\ \mathrm{cm^{-1}}$ and the anharmonicity constant $\omega_e x_e = 8.5(2)\ \mathrm{cm^{-1}}$ to be determined for NMA isolated in SMH samples with low oH_2 concentrations.
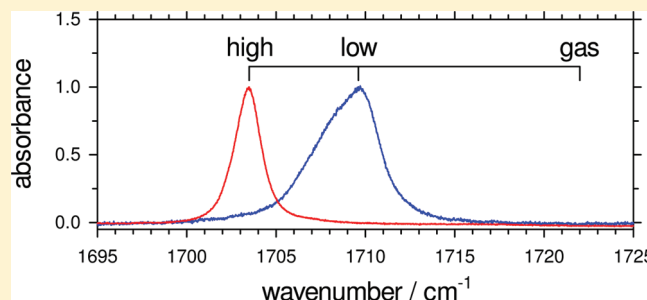
1. INTRODUCTION

There has been an extensive amount of experimental[1-11] and theoretical[12-26] research aimed at clarifying the relationship between the secondary structure of peptides and proteins in solution and the frequency, intensity, and width of the infrared (IR) amide I band. IR spectroscopic studies of the model compound, *N*-methylacetamide ($CH_3CONHCH_3$, NMA), allow the amide I vibration to be probed in the absence of interpeptide couplings, providing important information about the vibrational dynamics of an isolated peptide bond. The ultrafast community has studied the nonlinear IR spectroscopy of NMA in part to disentangle contributions to the static line shape from lifetime broadening and solvent-induced frequency shifts.[2,5,8] Recently, Kubelka and co-workers investigated the temperature dependence of both the frequency and intensity of the amide I mode of NMA (and small peptides) dissolved in a variety of organic solvents in order to quantify temperature-dependent effects that are independent of structural changes for the analysis of temperature-jump transient IR experiments.[10,11,25] These studies showed that nonstructural changes in the NMA amide I frequency and intensity are small but significant.[10,11] The static room temperature absorption spectra of NMA dissolved in dimethyl sulfoxide, acetonitrile, and 1,4-dioxane reveal broad (fwhm > 10 $\mathrm{cm^{-1}}$) roughly symmetric amide I features that shift to lower wavenumbers and broaden with increasing solvent polarity.[10,11] We were motivated by this work to investigate the homogeneous and inhomogeneous contributions to the amide I line shape for NMA solvated in solid molecular hydrogen (SMH) at cryogenic temperatures. The IR spectrum of NMA embedded in cryogenic matrices (Ar and N_2) has previously been reported;[27-29] however, none of these studies provide high-resolution information on the line shape of the amide I feature of NMA under high dilution conditions.

SMH is a quantum solid[30,31] and has many desirable properties for the high-resolution IR spectroscopy of embedded solute molecules.[32-34] The H_2 molecule represents a limiting case in terms of a nonpolar minimally perturbing solvent. The H_2 molecule is a homonuclear diatomic, and thus the lowest order electrostatic moment it possesses is a quadrupole moment ($Q = 2.17 \times 10^{-40}\ \mathrm{C\ m^2}$) and H_2 has a modest polarizability ($\alpha = 0.802 \times 10^{-24}\ \mathrm{cm^3}$).[35] Therefore, the solute–solvent intermolecular interactions at long-range will be dominated by dipole–quadrupole and dipole-induced dipole interactions which are typically quite weak. In addition, SMH is a translational quantum solid due to the large amplitude zero-point motions of the H_2 molecules around their equilibrium crystal lattice positions, such that SMH has properties between a solid and a liquid which make it advantageous to study embedded NMA molecules. One of the difficulties with the earlier Ar and N_2 matrix isolation studies of NMA was the existence of multiple peaks thought to be due to multiple trapping sites or conformations of NMA.[27,28] In the case of SMH, "site splitting" is minimized by the ability of the SMH sample to self-anneal.[32] Further, at these low temperatures, nuclear spin restrictions on the total H_2 wave function result in *para*-hydrogen (pH_2) and *ortho*-hydrogen (oH_2) molecules exclusively populating $J = 0$ and $J = 1$ rotational states, respectively. Since H_2 nuclear spin conversion in the absence of paramagnetic species is very slow, non-equilibrium distributions of oH_2 and pH_2 can be kinetically trapped in SMH.[30] For a pH_2 molecule in a $J = 0$ state, the quadrupole moment averages to zero, while for an oH_2 molecule in a $J = 1$ state, it survives rotational averaging. Thus, SMH samples can be synthesized
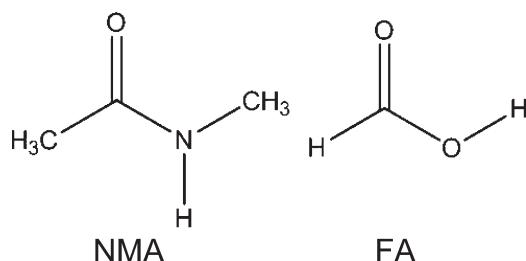
Figure 1. Kekule structures of *trans*-NMA and *trans*-FA.

with differing amounts of oH_2 to selectively probe how the stronger quadrupole—dipole electrostatic interactions perturb the NMA amide I spectrum.

In this work, we study the FTIR spectrum of the amide I mode of NMA in SMH matrices with low (0.03%) and high (55%) concentrations of oH_2. Our previous studies of formic acid (FA) isolated in SMH have shown that the frequency and line shape of the ν_3 carbonyl stretching mode of FA depends strongly on the oH_2 concentration in the sample.[36] At low oH_2 concentrations in highly enriched pH_2 solids, individual peaks are resolved for $FA(oH_2)_n$ clusters which form during deposition and annealing of the sample. These $FA(oH_2)_n$ clusters form in the solid because of stronger attractive interactions between FA and oH_2 due to the $J = 1$ rotational wave function of oH_2. For a pH_2 molecule, all anisotropic intermolecular interactions (such as dipole—quadrupole) average to zero for the $J = 0$ rotational wave function, while for oH_2 in a $J = 1$ rotational state, these interactions survive. This difference in J rotational state imposed by the total nuclear spin of the H_2 molecule leads to a small energetic preference for the oH_2 molecules to cluster to the polar FA dopant.[36]

On the basis of the similarities in the structures of NMA and FA (see Figure 1), that both contain the carbonyl moiety, we expect the amide I vibration of NMA and the ν_3 carbonyl stretching mode of FA to behave similarly in SMH matrices and to show a strong dependence on the oH_2 concentration within the sample. The present studies are aimed at quantifying the shift of the amide I mode frequency from its gas-phase value when NMA is solvated in SMH, the homogeneous width of the amide I fundamental which can be used to put a lower limit on the vibrational lifetime, and finally to directly measure the amide I overtone transition to better quantify the physical constants (ω_e and $\omega_e x_e$) of this important molecular vibration. These are important measures of the intrinsic vibrational dynamics of the NMA molecule or peptide bond that can serve as benchmarks for theoretical studies.

2. EXPERIMENTAL SECTION

The experimental apparatus used to synthesize and spectroscopically characterize chemically doped SMH matrices has been dutifully described.[36] Briefly, we utilize the rapid vapor deposition method of Fajardo and Tam,[37,38] whereby independent gas flows of H_2 and dopant are co-deposited onto a BaF_2 optical substrate cooled to ∼2.5 K in a sample-in-vacuum liquid helium cryostat (Janis SSVT-100). Room temperature normal hydrogen (nH_2) gas is precooled and enriched in the para-nuclear spin state during deposition using a home-built ortho/para (o/p) converter cooled by a separate closed-cycle helium cryostat (Advanced Research Systems CSW-204). In this work, two separate crystal depositions are conducted with the o/p

converter maintained at 14 and 80 K, respectively, to produce SMH samples with low (0.005%) and high (51.4%) concentrations of oH_2. These oH_2 concentrations are estimated using the rotational partition function of H_2 and assuming full thermal equilibration of the nuclear spin states at the temperature of the o/p converter.[36] We know from experience that in practice the low and high oH_2 concentration samples contain <0.03 and ∼55% oH_2, respectively.[39]

The NMA (Sigma-Aldrich, 99+%) is repeatedly freeze-pumped-thawed prior to use to remove volatile impurities. NMA has a vapor pressure of ∼0.075 Torr at 286 K, where the compound exists in the solid phase.[35] The FA (Sigma-Aldrich, ACS Reagent 88%) is present in the dopant vacuum manifold as an impurity due to earlier experiments with FA/O_2 mixtures conducted just days prior to the present experiments. We estimate the NMA and FA concentrations in the low oH_2 concentration SMH sample used to study the amide I fundamental to be 10 and 2 ppm based on the sample thickness determined from the peak absorbance of the $Q_R(0)$ feature at 4228.5 cm^{-1} using the correlation developed by Fajardo, and 209 and 231 km mol^{-1} absorption strengths for the amide I mode of NMA and the ν_3 mode of FA.[13,40] Similarly, for samples used to study the amide I overtone spectra, the NMA concentration is increased to approximately 40 parts per million (ppm).

The amide I fundamental absorption spectra recorded from 600 to 5000 cm^{-1} are obtained with a Fourier transform infrared (FTIR) spectrometer at a resolution of 0.05 cm^{-1} (nominal with boxcar apodization). The FTIR spectrometer (Bruker IFS 120 HR) is equipped with a globar source, a Ge-coated KBr beamsplitter, and a liquid nitrogen cooled HgCdTe detector for these experiments. Amide I overtone spectra are recorded using an InSb detector for improved S/N in the region around 3500 cm^{-1}. The entire optical path outside of the spectrometer and cryostat vacuum shroud is purged using a dry air generator (Domnick Hunter CO2RP850) to reduce atmospheric absorptions. So-called "as-deposited" spectra are recorded just after deposition is complete for samples that have never been exposed to temperatures greater than ∼2.5 K. The as-deposited samples are annealed by raising the temperature of the solid to 4.3 K for a specified period of time. In these experiments, we are concerned with spectral changes that occur with a slow time constant (∼1 h) after changing the temperature of the crystal. Accordingly, the measurement protocol followed is as follows; once a new temperature of the crystal is rapidly established, four repeated spectra are recorded with 376 s acquisition times (25 scans at 0.05 cm^{-1}) at 800 s delays to monitor changes in the spectra over approximately 1 h. A temperature range between 1.7 and 4.3 K is achieved by vacuum pumping on the helium in the bath cryostat. The temperature of the crystal is monitored (Lakeshore 331) with silicon diodes located at the cold tip (T_A) and at the base of the optical holder (T_B). All of the temperatures reported here are measured with T_B and are estimated to be good to within ±0.1 K in this temperature range.

3. RESULTS

In these studies, we co-deposit NMA and FA into SMH matrices at ppm concentrations for samples with low and high oH_2 concentrations and record high-resolution FTIR spectra at temperatures from 2 to 4 K. The FA molecule is used to help gauge the response of the NMA spectrum to the SMH matrix since we have previously studied the FA spectrum in detail.[36] We
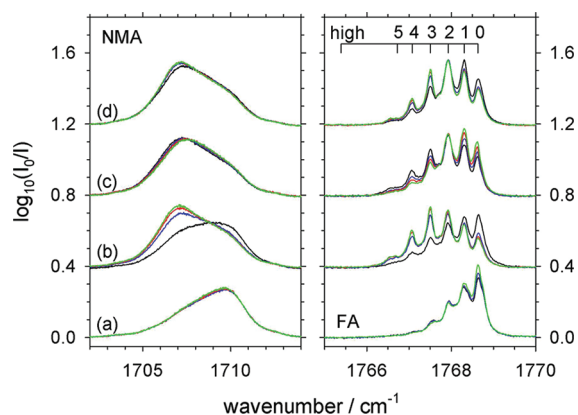
Figure 2. Series of IR spectra in the vicinity of the amide I mode of NMA near 1710 cm^{-1} and the ν_3 C=O stretching mode of FA at approximately 1768 cm^{-1} for a NMA/FA double-doped SMH sample with a low oH$_2$ concentration (0.03%). The four successive spectra recorded at 800 s delays for each trace (a–d) are color-coded with respect to time as follows: black, blue, red, and green. Trace (a) shows the four spectra recorded at 1.8 K for the as-deposited sample; trace (b) scans are recorded after raising the temperature to 4.3 K; trace (c) is recorded at 1.7 K after recooling; and trace (d) is recorded after raising the temperature back to 4.3 K. The FA(oH$_2$)$_n$ cluster frequencies are shown on the scale at the top, labeled by n the number of oH$_2$ molecules. The label "high" indicates the FA ν_3 frequency measured for FA isolated in SMH with 55% oH$_2$.

previously reported the spectrum NMA isolated in low oH$_2$ concentration SMH samples from 800 to 4000 cm^{-1} in collaboration with the Bouř research group.[41] In the current work, we focus on the details of the amide I mode spectrum of *trans*-NMA. The *trans* conformer (defined by the dihedral angle between the C=O and N–H bonds) is more stable[28] than the *cis* isomer by about 2.3 kcal/mol, and the *cis*-to-*trans* barrier is estimated to be 20 kcal/mol.[42] Therefore, the room temperature *cis* population likely gets frozen out in the SMH sample, but since it is predicted to be negligible (<2%),[42] we assume the amide I spectrum results solely from *trans*-NMA. Figure 2 presents a series of IR spectra in the region of the amide I mode of NMA near 1710 cm^{-1} and the ν_3 mode of FA at approximately 1768 cm^{-1} for a NMA/FA double-doped SMH sample with a low oH$_2$ concentration (0.03%). Trace (a) in Figure 2 shows four spectra recorded for the as-deposited sample at 1.8 K with an 800 s delay between each successive scan. The color coding in Figure 2 indicates the order in which the repeated scans were recorded, namely, black, blue, red, and green. The spectra in the region of the ν_3 mode of FA are consistent with our previous measurements[36] and show FA(oH$_2$)$_n$ cluster peak resolved structure for features with $n = 0$ to 5. The scale at the top of the FA ν_3 spectra indicates the cluster peak positions labeled by n, the number of oH$_2$ molecules in the cluster, as reported previously.[36] On the same scale, the peak position labeled "high" designates the FA ν_3 peak center measured for FA solvated in SMH with a 55% oH$_2$ concentration, as will be shown later. The first approximately five oH$_2$ molecules in the first solvation shell around the FA molecule shift the ν_3 vibrational frequency by an average value of −0.38 cm^{-1} per oH$_2$ molecule. Once this first solvation shell is complete, additional oH$_2$ molecules are further removed from the FA and the ν_3 vibrational frequency asymptotically approaches the value designated "high" with increasing oH$_2$ concentration.[36] Note that, for the as-deposited sample, the intensities of the FA(oH$_2$)$_n$ cluster

peaks change with time due to intracluster oH$_2 \rightarrow$ pH$_2$ nuclear spin conversion (NSC) which converts the larger clusters into smaller clusters. The NMA amide I peak shown in trace (a) is broad (∼5 cm^{-1}) and asymmetric with a sharp blue edge near 1710 cm^{-1}. Similar to the time-dependent changes observed for the ν_3 FA(oH$_2$)$_n$ cluster features, we observe the intensity of the NMA feature to increase near the blue edge with time.

We next raised the temperature of the sample to 4.3 K and similarly recorded four successive spectra with an 800 s delay between the start of each scan, and the observed spectra are shown in trace (b) of Figure 2. For rapid vapor-deposited SMH samples, the first time the temperature of the sample is raised to 4.3 K, the crystal anneals as evidenced by an irreversible growth in the FA(oH$_2$)$_n$ clusters. The rapid vapor deposition method produces well-isolated dopant species due to the rapid freezing of the matrix host during deposition and the properties of SMH.[43] Studies with polar dopant species such as HCl have shown that the HCl is well-isolated in as-deposited samples and only forms appreciable cluster species ((HCl)$_2$, (HCl)$_3$, etc.) when the sample is thermally annealed at 4.3 K.[44] Similarly, we observe that the FA(oH$_2$)$_n$ cluster distribution is always strongly weighted toward the smallest cluster sizes in the as-deposited sample and shifts irreversibly toward larger cluster sizes upon annealing. The cluster growth process is apparent in trace (b); the intensity of small FA(oH$_2$)$_n$ clusters features ($n = 0, 1$) decrease with time, while the intensity of larger cluster features ($n = 2$–5) increase. Thus, annealing the sample results in a net growth of FA(oH$_2$)$_n$ clusters until the systems reaches a new dynamic equilibrium. This can be seen in trace (b) where the intensity changes are initially large but become less and less with repeated scans such that the third and fourth scans are nearly superimposed on one another. Similar large changes in the NMA spectra are also observed upon annealing the as-deposited sample. In the case of NMA, intensity in the amide I mode shifts from regions of higher energy (∼1710 cm^{-1}) to lower energy (1707 cm^{-1}) such that the peak has the reverse asymmetry in the annealing sample compared to the as-deposited sample. Note that similar to the FA(oH$_2$)$_n$ cluster spectra, these changes in intensity decrease with time at the higher temperature.

Next, the sample is recooled to 1.7 K, and again, four spectra are recorded at 800 s delays; the resultant spectra are shown in trace (c). First, the spectra never completely return to what they looked like for the as-deposited sample. However, at low temperature, we observe that the FA(oH$_2$)$_n$ cluster distribution shifts with time toward smaller cluster sizes. This is evident in trace (c), where the intensity of the $n = 5, 4,$ and 3 cluster peaks decreases with time while the intensities of the $n = 1$ and 0 cluster peaks increase (the $n = 2$ peak intensity is nearly constant). This shift in the cluster distribution is caused by intracluster NSC, and these changes proceed with a slow rate constant ($k = 0.15(3)$ h^{-1}) such that the increase in the $n = 0$ feature is nearly linear with time in the four successive spectra recorded in approximately 1 h.[36] Similarly, we observe that the amide I feature for NMA decreases in intensity at the low energy side and increases on the high energy side, causing an apparent shift toward higher wavenumbers. Furthermore, these changes are proceeding with a slow rate constant and do not seem to be approaching a limiting value in the approximately 1 h time scale of the repeated scans.

The temperature of the sample is raised again to 4.3 K, and the recorded spectra are shown in trace (d). Note that similar to trace (b) there is an observed shift in the FA(oH$_2$)$_n$ cluster distribution toward larger cluster sizes. These changes are not as large and
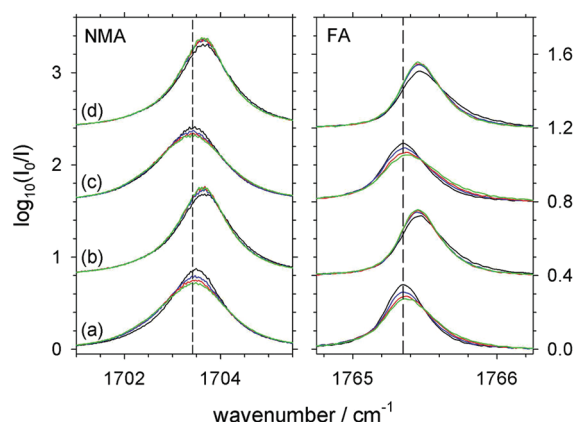
Figure 3. Series of IR spectra in the vicinity of the amide I mode of NMA near 1703 cm^{-1} and the ν_3 mode of FA at approximately 1765 cm^{-1} for a NMA/FA double-doped SMH sample with a high oH$_2$ concentration (55%). The four successive spectra recorded at 800 s delays for each trace (a−d) are color-coded with respect to increasing time as follows: black, blue, red, and green. Trace (a) shows the four spectra recorded at 2.0 K for the as-deposited sample; trace (b) is recorded after raising the temperature to 4.4 K; trace (c) is recorded at 1.9 K after recooling; and trace (d) is recorded after raising the temperature back to 4.3 K. The dashed lines indicate the peak center measured at low temperature for the annealed sample.

abrupt as the first time the as-deposited sample is annealed at 4.3 K, but nonetheless, the cluster distribution shifts toward larger cluster sizes as evidenced by the shift in intensity to lower wavenumber peaks. We take this as evidence that the oH$_2$ diffusion rate sufficiently increases from 1.7 to 4.3 K to account for this reversible component in the observed temperature dependence of the FA(oH$_2$)$_n$ cluster spectra.[45] The rate of intracluster NSC likely does not change much with temperature, and thus if the oH$_2$ diffusion rate increases at high temperature, then there should be a shift to larger oH$_2$ cluster sizes but these changes should diminish as the new equilibrium is established. Similarly, at high temperature, the NMA amide I peak shifts to lower energy, and these changes also diminish with time over the 1 h time scale of the repeated measurements.

On the basis of the similar behavior of the NMA amide I peak and the FA(oH$_2$)$_n$ ν_3 cluster features with temperature, time, and thermal history, we speculate that part of the breadth of the NMA amide I feature is caused by oH$_2$ clustering to the NMA molecule. However, unlike the case of the ν_3 mode of FA, individual cluster peaks are not resolved for the small $n = 0-5$ clusters but rather just a broad asymmetric peak is observed. This demonstrates that, while the NMA amide I spectrum is much narrower than room temperature spectra recorded in nonpolar liquid solvents,[10] the spectrum is not free of inhomogeneous broadening caused by varying numbers of oH$_2$ molecules in the first solvation shell of NMA. Since the individual cluster sizes are not resolved for NMA, the homogeneous width of NMA solvated in SMH with low oH$_2$ concentrations cannot be determined.

To further illustrate that the broadening of the NMA amide I mode in SMH is due at least in part to oH$_2$ clustering, another NMA/FA double-doped SMH sample is deposited with a much higher oH$_2$ concentration (55% oH$_2$). The resulting NMA amide I and FA ν_3 spectra are shown in Figure 3 for the analogous series of spectra shown in Figure 2. Trace (a) in Figure 3 shows four successive scans of the as-deposited sample revealing that, under

these conditions of high oH$_2$ concentration, the FA ν_3 peak maximum has shifted to approximately 1765.35 cm^{-1} at 2.0 K. In this case, the first and higher-order solvation shells of the FA dopant are expected to be occupied by oH$_2$ molecules such that the peak shifts to the red and sharpens compared to the analogous as-deposited feature measured for SMH with low oH$_2$ concentrations. At low oH$_2$ concentrations, the FA solvent environment is inhomogeneous as each FA molecule has a varying number of oH$_2$ molecules in the first solvation shell. These inhomogeneities are spectrally resolved for FA in the ν_3 mode, and the absorption consists of multiple partially overlapping peaks over an approximately 2.5 cm^{-1} range (see Figure 2). However, at high oH$_2$ concentrations, the complete first solvation shell of FA is filled with oH$_2$ molecules, leading to a more homogeneous environment in terms of the ortho/para make up; thus the ν_3 absorption collapses into a single symmetric feature. Similarly, while the NMA peak is broad and asymmetric for SMH samples with low oH$_2$ concentrations due to varying numbers of oH$_2$ clustered to NMA, in the 55% oH$_2$ SMH sample, the amide I peak shifts to lower wavenumbers and becomes sharper and symmetric.

As shown in Figure 3, repeated spectra recorded at 2.0 K for the as-deposited sample show that both the NMA amide I and FA ν_3 peaks broaden with time, indicating changes in the spectrum with a very slow characteristic time constant. When the sample temperature is raised to 4.4 K, the first scan shows that both the NMA and FA peaks have shifted to higher wavenumbers and sharpened. From inspection of traces (c) and (d) in Figure 3, these changes are completely reversible. The symmetric line shape of the NMA amide I absorption allows the peak position and width to be determined with high precision by least-squares fitting the data to an appropriate line shape function. In this case, the NMA amide I peak in each spectrum is fit to a pseudo-Voigt line shape of the form[46]

$$I(\tilde{\nu}) = fL(\tilde{\nu}) + (1-f)G(\tilde{\nu}) \tag{1}$$

$$L(\tilde{\nu}) = \frac{2A/\pi\gamma_0}{1 + 4\left(\dfrac{\tilde{\nu}-\tilde{\nu}_0}{\gamma_0}\right)^2} \tag{2}$$

$$G(\tilde{\nu}) = \frac{A}{\gamma_0}\sqrt{\frac{4\ln(2)}{\pi}}\exp\left[-4\ln(2)\left(\frac{\tilde{\nu}-\tilde{\nu}_0}{\gamma_0}\right)^2\right] \tag{3}$$

where $I(\tilde{\nu})$, $L(\tilde{\nu})$, and $G(\tilde{\nu})$ are the pseudo-Voigt, Lorentzian, and Gaussian line shape functions, and the fitting parameters f, A, γ_0, and $\tilde{\nu}_0$ represent the fractional contribution of the Lorentzian line shape, total peak area, the full width at half-maximum (fwhm), and the peak center, respectively.[46] Shown in Figure 4 are the results of fitting the pseudo-Voigt line shape to the NMA amide I feature at 1.9 and 4.3 K. The fitted parameters for these specific spectra are presented in Table 1. The NMA amide I feature is well fit by the pseudo-Voigt line shape, as shown by the residuals of the fit which are multiplied by 2 and plotted in Figure 4. At 1.9 K, the peak has a fwhm of 1.803(3) cm^{-1} and is 71.8(4)% Lorentzian. At 4.3 K, the peak sharpens with a fwhm of 1.258(2) cm^{-1} and the peak becomes 98.3(3)% Lorentzian. Note that the FA ν_3 peak center at 4.3 K determined from the fitted line shape 1765.4734(9) cm^{-1} agrees quantitatively with
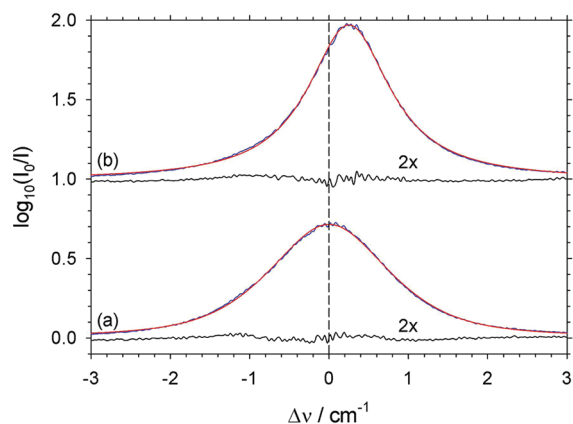
Figure 4. Results of fitting the amide I fundamental (blue) to a pseudo-Voigt line shape (red) for the line shapes recorded for NMA solvated in a SMH with 55% oH_2 at (a) 1.9 K and (b) 4.3 K. The residuals are multiplied by 2 and shown as black lines.

Table 1. Representative Fitted Pseudo-Voigt Parameters for NMA and FA in SMH with a High oH_2 Concentration (Uncertainties in Parentheses Are the 1σ Values Determined from the Fit)

	NMA		FA	
T (K)	1.92	4.35	1.92	4.35
A (cm^{-1})	1.803(3)	1.917(2)	0.1720(6)	0.1715(6)
fwhm (cm^{-1})	1.802(2)	1.258(2)	0.479(2)	0.341(1)
f	0.718(4)	0.983(3)	0.760(9)	0.758(9)
ν_0 (cm^{-1})	1703.3855(6)	1703.6357(4)	1765.4055(5)	1765.4734(4)

the 1765.5 cm^{-1} value reported by Räsänen and co-workers[47] for FA solvated in nH_2 at 4.2 K.

To better quantify the changes in the NMA amide I line shape with temperature and time, the fwhm and peak center determined from fitting the spectra to the pseudo-Voigt line shape are presented in Figure 5. Under conditions of high oH_2 concentration, the changes with temperature are almost completely reversible; however, changes with time can mask the temperature dependence. As shown in Figure 5, the fwhm steadily increases and the peak center shifts to lower wavenumbers with time for spectra recorded of the as-deposited sample at 2.0 K. These changes in fwhm are well fit by first-order kinetics, while the changes in peak center with time are more subtle. When the temperature is raised to 4.4 K for the first time, the peak shifts almost instantaneously to higher wavenumbers (+0.24 cm^{-1}) and then shifts slightly back (−0.04 cm^{-1}) with time. However, at high temperature, the changes in the NMA line shape are all complete within 1 h. In contrast, when the temperature of the sample is lowered to 1.9 K, the amide I feature starts to broaden with a slow first-order time constant (1.8(3) h^{-1}) such that even after 1 h changes are still occurring in the amide I line shape. Interestingly, when the temperature is quickly lowered, the peak shifts immediately to lower wavenumbers and then continues to shift to lower wavenumbers with time, but then after about 1 h starts to shift toward higher wavenumbers. We speculate that local NSC of oH_2 molecules solvated around the NMA dopant is responsible for these gradual changes in peak center and fwhm at low temperature.
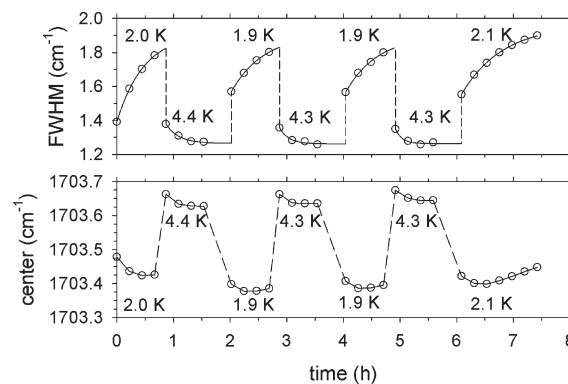
Figure 5. Plots of the fitted amide I fundamental peak center and fwhm for NMA isolated in SMH with 55% oH_2 as a function of temperature and time.
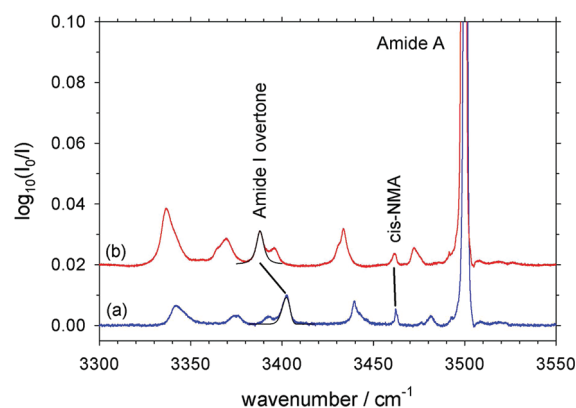

Figure 6. IR spectra in the vicinity of the amide A fundamental near 3500 cm^{-1} showing the peaks assigned to the amide I overtone of NMA solvated in SMH with low (a) and high (b) oH_2 concentrations. The amide A peak assigned to *cis*-NMA is also indicated.

To measure the overtone of the amide I mode, the NMA concentration is increased to 40 ppm and spectra are recorded with the InSb detector in the region around the amide A transition at 3500 cm^{-1}. Representative spectra for as-deposited samples synthesized with low and high oH_2 concentrations are shown in Figure 6. Multiple weak peaks are observed in this region. The peaks can be NMA combination bands or peaks due to NMA clustered with other trace species present in the sample (note these samples do not contain FA). One of these features can be assigned to the amide A transition of *cis*-NMA based on the shift observed for this vibration in previous measurements.[28] The spectrum is still relatively sparse, however, so that the amide I overtone can be assigned via inspection and the assignment tested using the measured line shape and further concentration studies. For the low oH_2 sample (trace (a) in Figure 6), the amide I overtone peak is observed at 3402.5 cm^{-1} and has an asymmetric line shape similar to the fundamental. For the high oH_2 concentration sample, the peak is observed at 3387.7 cm^{-1} and has a symmetric line shape, albeit significantly broader than the fundamental peak.

4. DISCUSSION

In this section, we will examine the vibrational shift and line shape of the amide I mode of NMA isolated in SMH in more
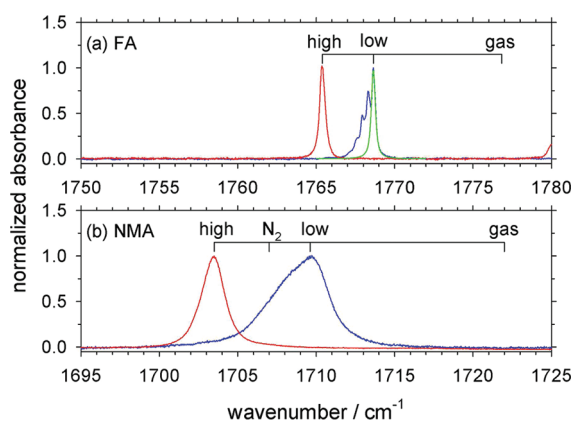
Figure 7. Representative absorption features of the ν_3 mode of FA (a) and amide I mode of NMA (b) isolated in SMH with low (blue) and high (red) oH$_2$ concentrations. Note that both the NMA and FA spectra are shown over an equivalent 30 cm^{-1} spectral range. The fitted line shape of the $n = 0$ FA(oH$_2$)$_n$ cluster feature is shown in green. The scale at the top indicates the peak centers with respect to the gas-phase value.

Table 2. Measured peak centers (cm^{-1}) for FA and NMA embedded in SMH. The percentage shifts from the gas-phase values are presented in parentheses

species	low [oH$_2$]	high [oH$_2$]	gas phase
FA ν_3(1←0)	1768.63 (−0.461%)	1765.41 (−0.643%)	1776.83[a]
NMA amide I (1←0)	1709.7 (−0.714%)	1703.4 (−1.08%)	1722[b]
NMA amide I (2←0)	3402.5 (−1.09%)	3387.7 (−1.52%)	3440[c]

[a] From ref 49. [b] From ref 12. [c] From ref 48.

detail. To aid this discussion, we show in Figure 7 spectra in the FA ν_3 and NMA amide I regions, respectively, for both SMH samples with low and high oH$_2$ concentrations, indicate the gas-phase frequencies for NMA and FA,[12,48,49] and present the measured peak center frequencies in Table 2.

(a). Vibrational Shifts of NMA in SMH. SMH is a unique solvent due in part to its quantum mechanical nature.[32−34] While it is crystalline with long-range order, the weak H$_2$−H$_2$ intermolecular forces and low H$_2$ molecular mass allow the solid to self-anneal even at low temperature.[32] Thus, the very low temperatures prevent the NMA molecules from diffusing and agglomerating, but significant translational zero-point energy in SMH minimizes defects and inhomogeneities in the NMA solvation environment. Further, since the H$_2$ molecules in SMH retain good rotational quantum numbers, the effects of isotropic and anisotropic H$_2$ intermolecular forces on the solute vibrational frequency can be probed separately. As discussed in the Introduction, all anisotropic intermolecular interactions average to zero for a spherically symmetric $J = 0$ rotational state. Thus, to the extent that the H$_2$ molecules in the first solvation shell around the NMA retain good rotational quantum numbers, the results for low and high oH$_2$ concentrations allow the isotropic and anisotropic H$_2$ contributions to be quantified. For FA, the shift in the center frequency due to isotropic forces (mainly dipole-induced dipole) in SMH samples with low oH$_2$ concentrations is −8.20 cm^{-1}, and anisotropic interactions (largely dipole−quadrupole) shift the peak an additional −3.22 cm^{-1}. The FA ν_3 peaks for low and high oH$_2$ concentration samples are shown in Figure 7 compared to the gas-phase vibrational origin.

Note, since the FA(oH$_2$)$_n$ cluster peaks are resolved at low oH$_2$ concentrations, the peak center and line width of the $n = 0$ cluster peak can be determined, and this peak is shown in green in Figure 7. For NMA, the corresponding shifts are −12.3 and −6.3 cm^{-1}, respectively, and thus anisotropic interactions are responsible for 50% more of a shift in the amide I band center. Unlike FA, the $n = 0$ peak of NMA cannot be determined in SMH samples with low oH$_2$ content since the cluster peaks are not resolved. However, we use the as-deposited sample as the best approximation to NMA embedded in pure pH$_2$ for the shift calculations and show an as-deposited NMA amide I spectrum in Figure 7 (blue trace). Quantitatively, the shift of the band center for the NMA amide I mode is 1.50 and 1.63 times larger than the corresponding shifts in the FA ν_3 mode. This begins to quantify the anomalous sensitivity the NMA amide I vibration has to solvent environment. It is interesting to compare the present results with those of Ataka for NMA solvated in solid N$_2$, where the N$_2$ molecules do not rotate freely. The N$_2$-solvated NMA amide I band center falls between the values for NMA in SMH with low and high oH$_2$ content, as shown in Figure 7 by the tick mark labeled N$_2$. For NMA solvated in SMH, the oH$_2$ molecules can optimize their (M_J) alignments with respect to the NMA dipole moment, while in solid N$_2$, close packing and repulsive N$_2$−N$_2$ interactions dominate, and therefore, the shift toward lower energy is less in solid N$_2$ than in SMH with a high oH$_2$ concentration.

The anomalous sensitivity of the amide I mode of NMA to the solvent environment can be traced to the unique electronic structure of the CONH peptide bond where NMA−solvent interactions can make it have more zwitterionic character and the intermolecular interactions can be relatively strong since they include hydrogen bonding.[12,18] In addition to the possibility of hydrogen bonding interactions, electrostatic effects are significant due to the large permanent dipole moment (3.68 D) of NMA and the large change in the dipole moment upon vibrational excitation of the amide I mode.[50] The vibrationally averaged dipole moments for NMA in the ground and amide I excited state have not been reported in the literature; however, the large IR oscillator strength associated with this mode (209 km/mol) indicates a significant increase in the dipole moment upon vibrational excitation.[13] In the case of NMA solvated in SMH with a low oH$_2$ concentration, the strongest NMA−H$_2$ attractive intermolecular force is a dipole-induced dipole interaction, and this type of induction force falls off with a $1/R^6$ dependence. In contrast, the NMA−H$_2$ intermolecular interaction with an oH$_2$ molecule, which has a rotationally averaged quadrupole moment, can interact via induction but also via the dipole−quadrupole electrostatic interaction which falls off with a $1/R^4$ dependence. Thus, any oH$_2$ molecules present in the first solvation shell of the NMA can interact more strongly with the NMA dopant which leads to a greater "reaction field" and a greater shift in the NMA amide I mode. A simple estimate based on the dipole−quadrupole interaction between an NMA molecule and an oH$_2$ molecule (with a $J = 1$ rotationally averaged quadrupole moment equal to 0.19441 au)[30] at a distance of 3.79 Å indicates that the dipole−quadrupole attractive interaction is approximately −70 cm^{-1}. This greater stability of the NMA−oH$_2$ pair is consistent with the experimental finding that oH$_2$ molecules preferentially solvate NMA at cryogenic temperatures.

(b). NMA Amide I Line Width. As pointed out in other IR line shape studies of molecules trapped in SMH with low oH$_2$ concentrations,[51−54] the line shape of the dopant species can

be incredibly sharp due to the minimally perturbing nature of the SMH host. For example,[55] IR studies of the ν_3 C–F stretching mode of CH_3F isolated in SMH with <300 ppm oH_2 concentrations reveal line shapes with a fwhm of <0.02 cm^{-1}. Typically, as the dopant or oH_2 concentration is increased, the dopant line shape broadens due to increased amounts of inhomogeneous broadening presumably due to long-range electrostatic interactions.[55] However, in the case of NMA, the fwhm of the amide I peak cannot be determined in SMH with low oH_2 concentrations because of inhomogeneous broadening caused by residual oH_2 present in the sample (see the blue trace in Figure 7). For FA, while this same inhomogeneous broadening mechanism is operative, the individual $FA(oH_2)_n$ cluster peaks are resolved so that the width of the $n = 0$ feature can be determined (green trace in Figure 7).[36] For NMA, this is not possible since the individual $NMA(oH_2)_n$ cluster peaks are not resolved, which means that the amide I fwhm can only be determined for NMA isolated in SMH samples with high oH_2 concentrations where inhomogeneous broadening due to dipole–quadrupole interactions are more prevalent, but inhomogeneities in the oH_2/pH_2 make up of the first solvation shell are much reduced.

Even for SMH with high oH_2 concentrations, however, inhomogeneous broadening is still very weak compared to typical solvents and conditions (e.g., water at room temperature). For this reason, homogeneous and inhomogeneous broadening mechanisms in SMH can both result in Lorentzian line shapes, and therefore, assigning Lorentzian widths solely to homogeneous broadening can be misleading.[36,54] However, in the limit of negligible inhomogeneous broadening, the observed fwhm must approach the line width determined by energy and phase relaxation.[52] This is typically expressed as

$$\gamma = \frac{1}{\pi c T_2} = \frac{1}{2\pi c T_1} + \frac{1}{\pi c T_2'} \tag{4}$$

where γ is the fwhm of the peak (in cm^{-1}), T_2 is the dephasing time, T_1 is the population relaxation time, and T_2' is the pure dephasing time. For frequency domain experiments the T_1 and T_2 contributions are typically determined by measuring the temperature dependence of the broadening, where at low temperature the pure dephasing time increases more rapidly with temperature than population relaxation.[51–54]

Usually the narrowest dopant IR line shapes are measured at the coldest temperatures for dilute concentrations of a dopant trapped in SMH with low oH_2 concentrations. The increase in the line width of the dopant IR transition with temperature over the range from around 2 to 10 K is interpreted as evidence that pure dephasing increases at higher temperatures due to thermal population of acoustic phonon modes in the sample.[51–54] For CD_4 isolated in SMH with low oH_2 content, detailed line shape measurements as a function of temperature allowed the fwhm of the ν_3 (2260 cm^{-1}) and ν_4 (996 cm^{-1}) vibrational modes to be determined to be 0.177 and 0.000 cm^{-1} at the 0 K limit, where the broadening is assumed to be due purely to population relaxation.[52] The large difference in the measured T_1 times (30 ps and >5300 ps) is presumably due in part to intramolecular vibrational redistribution, which is known from gas-phase measurements to be significant in the ν_3 fundamental mode and not in the lower energy ν_4 mode.

The excited vibrational state dynamics is different for NMA solvated in SMH with high oH_2 concentrations since the narrowest line shapes are measured at high temperature, not at low. This temperature effect can be rationalized as a sort of motional narrowing. The stronger NMA–oH_2 intermolecular interactions (dipole–quadrupole) lead to increased inhomogeneous broadening at low temperature where the M_J alignment of oH_2 molecules next to the NMA is more prevalent due to the Boltzmann weighting. In contrast, at high temperature, thermal fluctuations tend to wash out local anisotropic interactions and lead to a more isotropic environment. Motional narrowing is possible as long as the excited vibrational state is long-lived with respect to the rotational period of H_2, which for the light H_2 molecule is very short ($1/2B$ = 0.28 ps). In addition, thermal expansion of the solid can lead to less inhomogeneous broadening at higher temperatures just due to the increased intermolecular distance between NMA and the first H_2 solvation shell. Consistent with this interpretation, the NMA amide I peak shifts to higher wavenumbers or toward the gas-phase value with an increase in temperature, indicating the perturbations are less at high temperature. Further, the line shape changes to a more Lorentzian profile at the higher temperatures. Thus, we use the fwhm of the amide I mode recorded at high temperature as a lower limit to the vibrational lifetime.

The extracted widths from the NMA amide I peak spectra are used to calculate the lifetime of the excited state for NMA isolated in SMH assuming the relaxation is due to population decay. Simply using the average fwhm = 1.268(8) cm^{-1} measured over six separate spectra, a lower limit to the vibrational lifetime is determined to be 4.19(3) ps, which is short compared to the T_1 lifetimes extracted for CD_4 in SMH with low oH_2 content. The measured NMA amide I mode lifetime is also short compared to the ν_3 mode of FA which has a fwhm of 0.34 cm^{-1} under the same conditions yielding a 16 ps lifetime. This suggests that the anomalously short lifetime is a property of the NMA molecule and not solvent-dependent. Room temperature ultrafast IR pump–probe experiments have reported biexponential relaxation dynamics for NMA with 0.45 and 4 ps decay times, respectively.[2,5,8,26] The slower relaxation time is consistent with the lifetime determined in this study, while the fast component would only contribute to the baseline in static spectra and therefore cannot be observed here.

(c). Anharmonicity Constant for the Amide I Mode. The anharmonicity constant for the amide I mode of NMA in SMH is obtained using the measured fundamental and overtone frequencies and by defining the term values of the amide I vibration as

$$G(v) = \omega_e(v + 1/2) - \omega_e x_e(v + 1/2)^2 \tag{5}$$

from which ω_e = 1726.6(5) cm^{-1} and $\omega_e x_e$ = 8.5(2) cm^{-1} is obtained for NMA in SMH with a low oH_2 concentration as measured for the as-deposited samples at 1.8 K. The low oH_2 concentration data are used to determine the anharmonicity constant since these solids provide the minimum perturbations to the vibrational frequencies and thus should provide the best estimates for the physical constants of an isolated NMA molecule. These physical constants are consistent with previous resonance Raman measurements[48] and with the $2\omega_e x_e$ values determined in ultrafast IR pump–probe experiments.[2,5,8] On the basis of these assignments and line shape fits to the data, the amide I overtone peak is 112(1) times weaker and 2.7(1) times broader than the fundamental.

5. CONCLUSIONS

The high-resolution (0.05 cm^{-1}) IR absorption spectrum of the amide I mode of NMA isolated in SMH with low and high

oH_2 concentrations is presented. Through double-doping experiments of NMA and FA, we demonstrate that the inhomogeneous broadening mechanism originally observed for the carbonyl stretching mode of FA isolated in SMH is also operative for the amide I mode of NMA. Namely, for SMH samples with low oH_2 concentrations, clustering of small numbers of oH_2 molecules to the dopant molecule results in inhomogeneous broadening of the peak. Furthermore, since the attractive intermolecular interactions between NMA$-oH_2$ are greater than NMA$-pH_2$, preferential solvation by oH_2 is observed even for SMH samples with exceedingly low oH_2 concentrations (<300 ppm). Consistent with the greater interaction between NMA and oH_2, the amide I peak center shifts to lower wavenumbers with increased oH_2 content. Comparison of the shifts of the peak centers for the carbonyl stretches of FA and NMA shows that the amide I mode of NMA is significantly more sensitive to solvent environment displaying shifts that are 1.5 to 1.6 times greater than FA. This anomalous sensitivity can be traced to the unique electronic structure of the peptide bond (CONH) and can be understood simply based on the Lewis dot structure and the concept of resonance.

One of the original goals of this work was to measure the homogeneous line width of the amide I mode of NMA in highly enriched pH_2 solids to provide further evidence that the fast vibrational relaxation dynamics observed in room temperature experiments is intrinsic to amide I mode and not strongly influenced by solvent polarity even under the extremely nonphysiological conditions of solvation in cryogenic SMH. However, we quickly found that the homogeneous width could not be determined due to unresolved inhomogeneous broadening of the peak under these conditions. To overcome this difficulty, we purposely increased the oH_2 concentration to around 55% such that now the NMA molecule has all oH_2 molecules in its first solvation shell, such that at 4.3 K the peak sharpened to approximately 1.268(8) cm^{-1} and is well fit by a Lorentzian line shape. The overall shift in the peak center of the amide I mode from its gas-phase value is larger in SMH with high oH_2 concentrations as compared to low, indicating stronger solute$-$solvent interactions, but the peak is no longer noticeably inhomogeneously broadened. This allows us to set a lower limit of 4.19(3) ps for the amide I vibrational lifetime of NMA isolated in SMH, demonstrating fast vibrational relaxation. Finally, we were also able to measure the amide I overtone peak and quantify the vibrational constants for NMA trapped in SMH.

■ ASSOCIATED CONTENT

ⓈSupporting Information. Survey IR spectrum recorded at 1.8 K of NMA in SMH with a low oH_2 concentration, table of all measured NMA transitions, series of repeated scans showing the effect of repeated temperature cycling on the NMA and FA$(oH_2)_n$ spectra. This material is available free of charge via the Internet at http://pubs.acs.org.

■ AUTHOR INFORMATION

Corresponding Author
*E-mail: danderso@uwyo.edu.

■ ACKNOWLEDGMENT

■ REFERENCES

(1) Krimm, S.; Bandekar, J. *J. Adv. Protein Chem.* **1986**, *38*, 181.

(2) Hamm, P.; Lim, M.; Hochstrasser, R. M. *J. Phys. Chem. B* **1998**, *102*, 6123.

(3) Manas, E. S.; Getahun, Z.; Wright, W. W.; DeGrado, W. F.; Vanderkooi, J. M. *J. Am. Chem. Soc.* **2000**, *122*, 9883.

(4) Asplund, M. C.; Zanni, M. T.; Hochstrasser, R. M. *Proc. Natl. Acad. Sci. U.S.A.* **2000**, *97*, 8219–8224.

(5) Zanni, M. T.; Asplund, M. C.; Hochstrasser, R. M. *J. Chem. Phys.* **2001**, *114*, 4579.

(6) Barth, A.; Zscherp, A. *Q. Rev. Biophys.* **2002**, *35*, 369.

(7) DeCamp, M. F.; DeFlores, L.; McCracken, J. M.; Tokmakoff, A.; Kwac, K.; Cho, M. *J. Phys. Chem. B* **2005**, *109*, 11016.

(8) Deflores, L. P.; Ganim, Z.; Ackley, S. F.; Chung, H. S.; Tokmakoff, A. *J. Phys. Chem. B* **2006**, *110*, 18973.

(9) Schweitzer-Stenner, R. *Vib. Spectrosc.* **2006**, *42*, 98.

(10) Amunson, K. E.; Kubelka, J. *J. Phys. Chem. B* **2007**, *111*, 9993.

(11) Ackels, L.; Stawski, P.; Amunson, K. E.; Kubelka, J. *Vib. Spectrosc.* **2009**, *50*, 2.

(12) Kubelka, J.; Keiderling, T. A. *J. Phys. Chem. A* **2001**, *105*, 10922.

(13) Watson, T. W.; Hirst, J. D. *J. Phys. Chem. A* **2002**, *106*, 7858.

(14) Watson, T. W.; Hirst, J. D. *J. Phys. Chem. A* **2003**, *107*, 6843.

(15) Kwac, K.; Cho, M. *J. Chem. Phys.* **2003**, *119*, 2247.

(16) Ham, S.; Kim, J.-H.; Lee, H.; Cho, M. *J. Chem. Phys.* **2003**, *118*, 3491.

(17) Bour, P.; Keiderling, T. A. *J. Chem. Phys.* **2003**, *119*, 11253.

(18) Besley, N. A. *J. Phys. Chem. A* **2004**, *108*, 10794.

(19) Torii, H. *J. Phys. Chem. A* **2004**, *108*, 7272.

(20) Bour, P.; Michalik, D.; Kapitán, J. *J. Chem. Phys.* **2005**, *122*, 144501.

(21) Hayashi, T.; Zhuang, W.; Mukamel, S. *J. Phys. Chem. A* **2005**, *109*, 9747.

(22) Bounouar, M.; Scheurer, C. *Chem. Phys.* **2006**, *323*, 87.

(23) Fujisaki, H.; Yagi, K.; Hirao, K.; Straub, J. E. *Chem. Phys. Lett.* **2007**, *443*, 6.

(24) Schultheis, V.; Reichold, R.; Schropp, B.; Tavan, P. *J. Phys. Chem. B* **2008**, *112*, 12217.

(25) Kaminsky, J.; Bour, P.; Kubelka, J. *J. Phys. Chem. A* **2011**, *115*, 30.

(26) Wang, L.; Middleton, C. T.; Zanni, M. T.; Skinner, J. L. *J. Phys. Chem. B* **2011**, *115*, 3713.

(27) Fillaux, F.; De Loze, C. *Chem. Phys. Lett.* **1976**, *39*, 547.

(28) Ataka, S.; Takeuchi, H.; Tasumi, M. *J. Mol. Struct.* **1984**, *113*, 147.

(29) Torii, H.; Tatsumi, T.; Kanazawa, T.; Tasumi, M. *J. Phys. Chem. B* **1998**, *102*, 309.

(30) Silvera, I. F. *Rev. Mod. Phys.* **1980**, *52*, 393.

(31) Van Kranendonk, J. *SOLID HYDROGEN: Theory of the Properties of Solid H₂, HD, and D₂*; Plenum Press: New York, 1983.

(32) Momose, T.; Shida, T. *Bull. Chem. Soc. Jpn.* **1998**, *71*, 1.

(33) Yoshioka, K.; Raston, P. L.; Anderson, D. T. *Int. Rev. Phys. Chem.* **2006**, *25*, 469.

(34) Bahou, M.; Huang, C.-W.; Huang, Y.-L.; Glatthaar, J.; Lee, Y. P. *J. Chin. Chem. Soc.* **2010**, *57*, 771.

(35) Lide, D. R., Ed. *CRC Handbook of Chemistry and Physics*, 82nd ed.; CRC Press LLC: Boca Raton, FL, 2001.

(36) Paulson, L. O.; Anderson, D. T. *J. Phys. Chem. A* **2009**, *113*, 1770.

(37) Fajardo, M. E.; Tam, S. *J. Chem. Phys.* **1998**, *108*, 4237.

(38) Tam, S.; Fajardo, M. E. *Rev. Sci. Instrum.* **1999**, *70*, 1926.

(39) Raston, P. L.; Kettwich, S. C.; Anderson, D. T. *Low Temp. Phys.* **2010**, *36*, 495.

(40) Yokoyama, I.; Yoshihisa, M.; Machida, K. *J. Am. Chem. Soc.* **1991**, *113*, 6458.

(41) Andrushchenko, V.; Matejka, P.; Anderson, D. T.; Kaminsky, J.; Hornicek, J.; Paulson, L. O.; Bour, P. *J. Phys. Chem. A* **2009**, *113*, 9727.

(42) Mantz, Y. A.; Branduardi, D.; Bussi, G.; Parrinello, M. *J. Phys. Chem. B* **2009**, *113*, 12521.

(43) Ceponkus, J.; Uvdal, P.; Nelander, B. *J. Phys. Chem. A* **2010**, *114*, 6829.

(44) Anderson, D. T.; Hinde, R. J.; Tam, S.; Fajardo, M. E. *J. Chem. Phys.* **2002**, *116*, 594.

(45) Meyer, H. *Low Temp. Phys.* **1998**, *24*, 381.

(46) Stancik, A. L.; Brauns, E. B. *Vib. Spectrosc.* **2008**, *47*, 66.

(47) Marushkevich, K.; Khriachtchev, L.; Rasanen, M. *Phys. Chem. Chem. Phys.* **2007**, *9*, 5748.

(48) Mayne, L. C.; Hudson, B. *J. Phys. Chem.* **1991**, *95*, 2962.

(49) Freytes, M.; Hurtmans, D.; Kassi, S.; Lievin, J.; Vander Auwera, J.; Campargue, A.; Herman, M. *Chem. Phys.* **2002**, *283*, 47.

(50) Kang, Y. K. *J. Mol. Struct.* **2001**, *546*, 183.

(51) Kerr, K. E.; Momose, T.; Weliky, D. P.; Gabrys, C. M.; Oka, T. *Phys. Rev. Lett.* **1994**, *72*, 3957.

(52) Katsuki, H.; Momose, T. *Phys. Rev. Lett.* **2000**, *84*, 3286.

(53) Kuroda, K.; Koreeda, A.; Takayangi, S.; Suzuki, M.; Hakuta, K. *Phys. Rev. B* **2003**, *67*, 184303.

(54) Toda, N.; Mizoguchi, A.; Kanamori, H. *J. Chem. Phys.* **2010**, *132*, 234504.

(55) Yoshioka, K.; Anderson, D. T. *J. Chem. Phys.* **2003**, *119*, 4731.

13667

dx.doi.org/10.1021/jp204800c |*J. Phys. Chem. B* 2011, 115, 13659–13667